LETTERS
PUBLISHED ONLINE: 19 FEBRUARY 2012 | DOI: 10.1038/NGEO1404
nature geoscience

Geomagnetic field variability during the Cretaceous Normal Superchron

Roi Granot*†, Jérôme Dyment and Yves Gallet

Prolonged periods of stable polarity in the Earth's magnetic field are termed superchrons. The most recent of these intervals, the Cretaceous Normal Superchron, lasted from approximately 121 to 83 million years ago[1,2] and is most commonly observed in the lack of a prominent stripe pattern[3] in the sea-surface magnetic anomaly above the oceanic crust formed during this period. The exact behaviour of the geomagnetic field during this interval, however, remains unclear, as palaeomagnetic data from igneous[4–6] and sedimentary[7,8] sections yield conflicting results. Here we report a deep-tow magnetic profile from the Central Atlantic Ocean, African flank, spanning the entire Cretaceous Normal Superchron. We suggest that this profile, along with widely distributed sea-surface magnetic anomaly data, records the rising variability of the dipolar geomagnetic field at the beginning of the interval, which culminates in a highly fluctuating field between 110 and 100 million years ago. We interpret the subdued magnetic signal in the last 9 million years of the superchron as the return to a more stable geomagnetic field. This variability allows us to define two internal time markers valuable for plate reconstructions. Based on the degree of variability observed, we conclude that geodynamo models that call for low field variability may provide an oversimplified view of superchrons.

Convective motions in the liquid-metal outer core of the Earth generate its magnetic field in a process known as the geodynamo. The long-term behaviour ($>10^5$ yr) of the geodynamo is generally believed to be strongly influenced by the thermal and compositional conditions imposed at the core–mantle boundary by mantle convection processes[9]. How the field evolved over a million-year timescale is arguably best illustrated by observing the frequency at which polarity reversals took place. Past variations in the strength of the dipole field offer additional important constraints on the evolution of the geodynamo. However, despite extensive palaeomagnetic work[4–8,10], little is known on the nature of the Cretaceous Normal Superchron (CNS). We therefore focused our efforts on investigating the magnetization of the CNS-age oceanic crust (defining the so-called 'Cretaceous quiet zone').

When magma rises at spreading ridges and cools, it acquires a thermoremanent magnetization proportional to the strength and parallel to the direction of the ambient geomagnetic field. Coherence between marine magnetic profiles[11,12] and correlation of these profiles with independent palaeomagnetic records[13–15] indicate that the oceanic crust is an efficient recorder of past secular variation of the dipole moment. We therefore collected a series of sea-surface magnetic and multichannel seismic reflection profiles across the quiet zone of the Central Atlantic Ocean, African flank, between the Kane and Atlantis fracture zones (Fig. 1a). Most importantly, we collected a total-field deep-tow magnetic profile (~1,000 m above the sea floor), encompassing the entire quiet zone; this profile provides a high-resolution 950-km-long record of crustal magnetization. Comparison between these data and sea-surface profiles from the conjugate flank and other widely separated oceanic basins (Fig. 2) reveals a similar pattern of magnetic anomalies, which indicates a geomagnetic field origin.

As is the case for most oceanic basins, spreading during the CNS in the Central Atlantic is marked both by ridge reorganization and asymmetric spreading[16,17]. South of the Atlantis fracture zone, full spreading rates evolved from 26 mm yr^{-1} before the CNS (anomalies M4y to M0) to 44 mm yr^{-1} immediately after the CNS (anomalies C34 to C33r). Asymmetry evolved from slightly faster spreading rates on the African flank during the early CNS to significantly faster rates on the North American flank during the late CNS. To assign ages along our deep-tow profile, we constructed a spreading-rate model by using calibration points given by the ages of the oldest sediments found immediately above the basalts in two Deep Sea Drilling Project (DSDP) drill holes and a distinctive magnetic anomaly found in conjugate positions on both flanks (see Supplementary Information). Change in the trend of fracture zones between ~95 and ~88 millionyears (Myr) ago was accompanied locally by an eastward ridge jump of up to 30 km (ref. 17; Fig. 1a). As a result, variable time intervals of up to 1.5 Myr in length are missing (African flank) or doubled (North American flank) in the magnetic records. We note, however, that our deep-tow profile is located in a spreading corridor that does not exhibit a significant spreading asymmetry during the CNS (Fig. 1a) and therefore probably provides a complete and regular magnetic record of the CNS.

To take into account the basement topography (considered as the top of the magnetized layer), which is partly hidden by the sedimentary cover, and the uneven track of the deep-tow profile, we inverted the deep-tow data to obtain an estimate of how magnetization evolved during the CNS (Fig. 1d, see Methods). The decreasing thickness of the sedimentary sequence towards the young end of the quiet zone (Supplementary Fig. S3) results in an increasing resolution of the deep-tow anomaly, from wavelengths of ~2 km (equivalent to ~0.13 Myr) at the beginning of the CNS to ~1 km (~0.05 Myr) at the end. Wavelengths greater than 50 km (~3.2 Myr and ~2.3 Myr at the beginning and end of the superchron, respectively) are unconstrained. Therefore, our deep-tow record resolves anomalies with wavelengths between ~2 and 50 km (~0.1 and ~2.3 Myr). The fluctuations of crustal magnetization increased gradually both in frequency and amplitude during the first 10 Myr of the superchron, with a maximum between 110 and 100 Myr ago. The frequency range widened from ~(0.3–2 Myr^{-1}) to ~(0.3–10 Myr^{-1}), and the magnetization contrast increased from ~5 to ~8 A m^{-1} (modelled magnetization values assume a 1-km-thick magnetic source layer; Supplementary Fig. S4). The frequency range narrowed and the magnetization contrast decreased after ~100 Myr ago to ~(0.3–1.3 Myr^{-1}) and

Institut de Physique du Globe de Paris, Sorbonne Paris Cité, Université Paris Diderot, UMR CNRS 7154, 1 rue Jussieu, 75238 Paris 05, France. †Present address: Department of Geological and Environmental Sciences, Ben-Gurion University of the Negev, Beer-Sheva 84105, Israel. *e-mail: rgranot@bgu.ac.il.

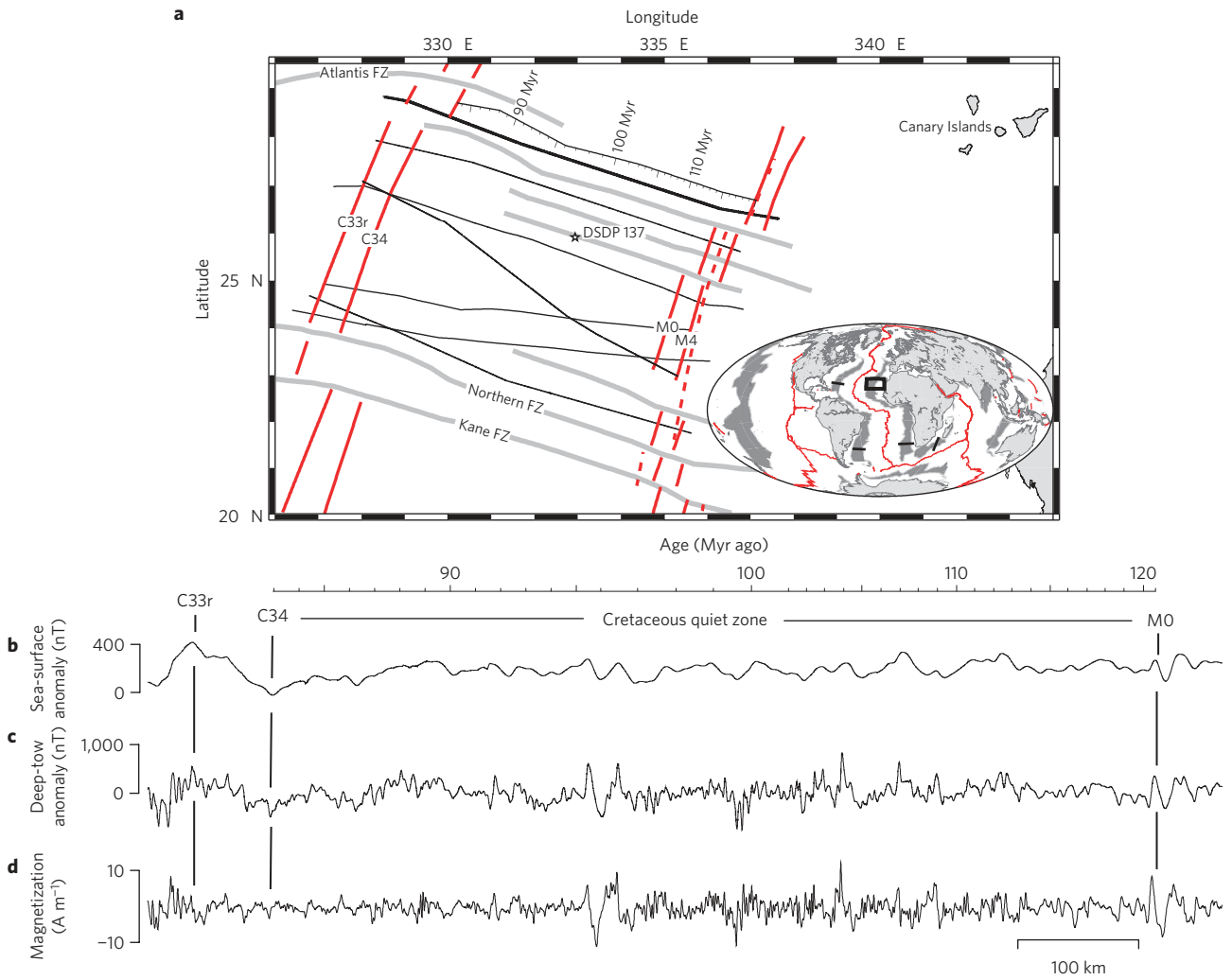

Figure 1 | Location map and deep-tow magnetic results. a, Location of deep-tow (thick black line) and sea-surface (thin black lines) profiles. Isochrons are shown with red lines, whereas dashed red lines delineate the location of the reconstructed C34 isochron restored to M0 isochron by a rotation of 12.88° about a pole at 55.25° N 350.0° E (based on ref. 17). Ages are based on the spreading model. Grey lines mark the fracture zones (FZ). Star indicates location of DSDP site 137. Inset: box shows the location of the studied areas. Black lines delineate the location of sea-surface profiles shown in Fig. 2. Cretaceous quiet zones are shown in dark grey. **b**–**d**, Sea surface (**b**), deep tow (**c**) and magnetization (**d**) of the profile straddling the corridor south of the Atlantis fracture zone. Magnetization was calculated assuming a uniform, 1-km-thick magnetic source layer (using the direct inversion method of ref. 28). The parameters used to calculate the inversion solution are specified in the Methods.

$\sim$5 A m^{-1}, respectively. The anomaly pattern cannot be attributed to the topographic variations of the magnetic source layer, as the predicted anomalies are far smaller in amplitude than the observed ones (Supplementary Fig. S3). The source of these anomalies could arise either from crustal construction processes (for example, variable magma supply leading to fluctuations in iron content and/or the thickness of the magnetic source layer) or from temporal changes of the geomagnetic field.

Fluctuations of the dipolar geomagnetic field generate a coherent magnetic anomaly signature in different spreading segments and oceanic basins. Comparison between representative sea-surface profiles from the South Atlantic, the Southwest Indian Ridge and, to a lesser extent, the Central Atlantic reveals similar anomaly patterns marked by an increase in anomaly amplitudes during the initial part of the superchron, followed by a period of high amplitude wiggles between 110 and 100 Myr ago (Fig. 2b–f). Thereafter, there was a decrease in amplitudes, which resulted in the highly subdued magnetic signature that characterizes the last $\sim$9 Myr of the CNS, in agreement with the deep-tow inversion solution. The more variable anomaly pattern shown by the Central Atlantic profiles (Fig. 2b–c) may be related to the formation of the Central Atlantic Basin at a slow-spreading ridge where crustal construction processes generated anomalies equal in size to the geomagnetic field signature, whereas the more regular anomaly pattern in the South Atlantic Basin and the Southwest Indian Ridge probably reflects their faster spreading rates during the CNS. In light of the above findings, we conclude that changes in the dipolar geomagnetic field were the main cause of the anomaly fluctuations pattern that we observe in both the deep-tow and the sea-surface data.

Our results constrain the short-term (between $\sim$0.1 and $\sim$2.3 Myr) fluctuations of the dipolar geomagnetic field during the CNS and reveal a long-term pattern of increase and decrease in its variability (Fig. 3 and Supplementary Fig. S4). We cannot rule out the presence of short reversed-polarity intervals, such as the ISEA event[8] in the early part of the CNS, as the altitude of our deep-tow profile and the slow spreading rate prevent the unambiguous detection of polarity intervals shorter than $\sim$0.1 Myr. Longer intervals of reversed polarity would result in standard oceanic anomalies that are absent in the quiet zone record. As only one reversed-polarity interval (ISEA) has so far been reliably detected, the observed

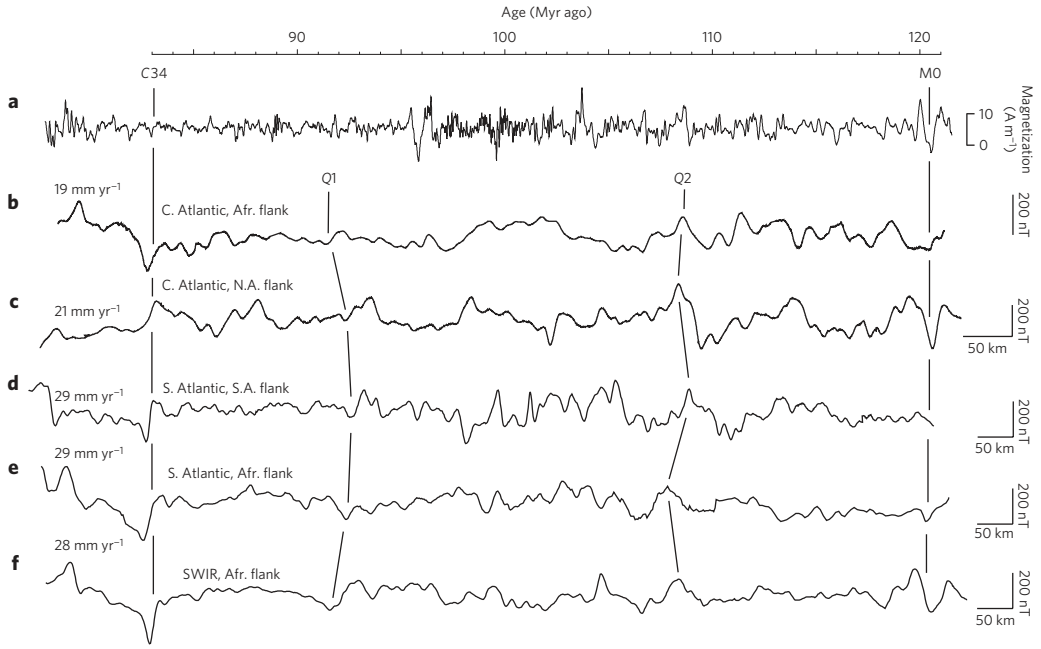

Figure 2 | Comparison of inverted deep-tow profile and widely distributed sea-surface magnetic anomalies. a, Magnetization inverted from the deep-tow magnetic profile (Fig. 1d). **b**–**f**, Representative sea-surface magnetic anomaly profiles from the Central Atlantic, African flank (**b**) and North American flank (**c**), South Atlantic, South American flank (**d**) and African flank (**e**), and Southwest Indian Ridge, African flank (**f**) are normalized based on the amplitudes of anomaly C34. Stretching of all the profiles to a common width is based on anomalies C34 and M0. The profiles shown in **a** and **b** were horizontally adjusted within the quiet zone for linear increase of ages. Half spreading rates are calculated between anomalies C34 and M0.

magnetic anomalies arise mainly from intensity fluctuations. From the amplitude envelope of the inverted deep-tow magnetic anomalies, we estimate the range of magnetization contrasts (Fig. 3a and Supplementary Fig. S4) to vary between up to ~4–5 A m^{-1} at the edges and ~8 A m^{-1} in the middle of the quiet zone, which indicates a higher variability of the geomagnetic field during the middle part of the CNS and a more stable field at the beginning and end of the superchron. The contrasts of magnetization deduced for the middle of the quiet zone are of the same magnitude as those resulting from typical reversal[18]. Conversely, deep-tow magnetic profiles across chrons C1 (Brunhes; ref. 13) and C5 (ref. 19) reveal magnetization contrasts of similar amplitude to those we obtained for the beginning and the end of the superchron (~5 A m^{-1}), which suggests that the variability of the geomagnetic field evolved from a standard reversing regime behaviour at the beginning and the end, to a highly fluctuating state in the middle of the superchron.

Comparison between the envelope of magnetic contrasts and the available palaeointensity data (Fig. 3) indicates some similarity between the beginning and the end of the superchron, when the dipole moment is well constrained and shows reduced variability. This observation is also supported by the remanent magnetization of two overlapping sedimentary sections in the Umbria–Marche area in central Italy[7], which indicates that subdued variability of relative palaeointensity prevailed between ~90 and 85 Myr ago. The palaeointensity data from the middle part of the CNS, when the field was most variable, are unfortunately too sparse to reliably demonstrate the expected field behaviour (Fig. 3b). However, it is worth noting that the magnetic anomalies of fracture zones from the North Pacific quiet zone[20] hint that the variability of the dipole moment during the middle part of the superchron was larger than that during the late part. Taken together, the above data further support the view that the geomagnetic dipole moment was more variable during the middle part of the CNS than at the beginning or the end of the superchron.

In light of our interpretation of the magnetic anomaly profiles in terms of geomagnetic field variability, we no longer envisage

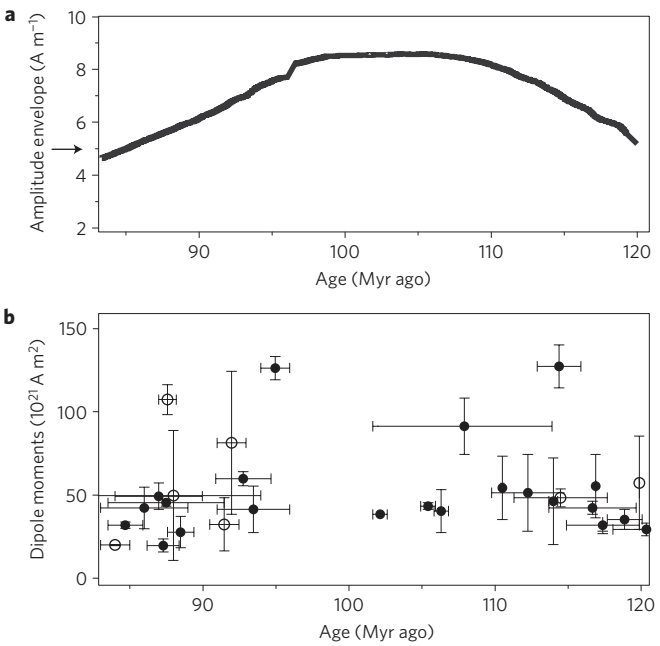

Figure 3 | Comparison of geomagnetic field variability during the CNS. **a**, Best-fit amplitude envelope of magnetic contrasts from the inverted deep-tow profile (1-km-thick magnetic source layer). Arrow indicates the typical amplitude envelope of magnetic contrasts from chrons C1 (Bruhnes; ref. 14) and C5 (ref. 20). **b**, Virtual axial dipole moments (open circles) and virtual dipole moment (filled circles) are site means and standard errors from the global absolute palaeointensity database[30] (http://earthref.org/magic/; see Supplementary Information).

the dipole as being very stable during the CNS, as previously considered solely on the basis of the polarity record, but rather as bearing significant and evolving intensity variations. Additional

palaeointensity data for the middle part of the CNS would be essential to constrain the relationship between the averaged dipole moment and its variability[21]. Numerical models of the geodynamo indicate that the distribution of the heat flux along the core–mantle boundary plays a key role in the initiation of superchrons[9,22] and predict that during the superchrons the field should tend to smaller variability and higher dipole moments than at times of frequent reversals. However, as these models consider uniform properties of the field within each polarity interval, we feel they fail to predict the long-term trend of variability throughout the CNS that can be seen from marine anomaly data. In our opinion, the models provide an oversimplified view of superchrons.

The history of seafloor spreading is a key factor controlling the shape of the oceanic basins and the evolution of sea-level height. Hence, the long-lasting global sea level highstand of the Middle Cretaceous[23] is believed to result from plate tectonic processes[24,25]. The lack of polarity reversals during the CNS prevents isochron identification, and therefore both the ages of major tectonic events and the evolution of spreading rates[26] are still poorly constrained during this period. Based on our results, we can define two internal time markers (Q1 and Q2, 92 and 108 Myr ago, respectively; Fig. 2) that can be used to date the oceanic crust, calculate plate kinematic models and provide important constraints on the evolution of the oceanic basins during the Cretaceous period.

Methods

Multichannel seismic reflection, sea-surface and deep-tow magnetic data were collected during a series of cruises aboard the RV *Le Suroît* of IFREMER, the French Research Institute for Exploitation of the Sea (cruises Magofond 3 and 3b in 2005 and 2008, respectively). These data were augmented with sea-surface magnetic data obtained from the National Geophysical Data Center database. For data analysis, we selected profiles spanning the entire quiet zone and near parallel (<45°) to the bounding fracture zones (see Supplementary Information for a complete discussion).

Seismic reflection data were acquired with a 400-m streamer and recorded by 24 hydrophones. Seismic-wave energy was produced by two synchronized air guns with a total volume of 150 cubic inches (2.5 l), shot every 40 m. Processing of the data included shot gather, normal move out, stacking and F–K (frequency–wavenumber) migration. Hand picking of basement-sediments contact was carried out with Kingdom Suite software. Conversion from time to depth was carried out with an average sediment velocity of 1.8 km s^{-1}.

Before inverting the deep-tow profile, we corrected the magnetic data for the effect of external magnetic field variation using the average data from the nearest two magnetic observatories, M'bour (Senegal), and Guimar (Canary Islands), and corrected for internal field using the IGRF 11 model[27]. We inverted[28] the uneven track of the deep-tow magnetic profile to calculate the equivalent magnetization of the upper 1 km considered to be the magnetic source layer. We removed unconstrained wavelengths greater than 50 km by filtering. Other parameters of the inversion solution were: azimuth of 110°; present inclination and declination of 39°/350°; remanent inclination and declination of 52°/320° based on the average location of the 80- and 120-Myr-old African palaeomagnetic poles from ref. 29. We note that the contributions of both the external field corrections and the uneven inversion method to the computed magnetization were negligible.

Received 7 July 2011; accepted 19 January 2012; published online 19 February 2012

References

1. Cande, S. C. & Kent, D. V. Revised calibration of the geomagnetic polarity timescale for the Late Cretaceous and Cenozoic. *J. Geophys. Res.* **100,** 6093–6095 (1995).
2. He, H. Y., Pan, Y. X., Tauxe, L., Qin, H. F. & Zhu, R. X. Toward age determination of the M0r (Barremian-Aptian boundary) of the Early Cretaceous. *Phys. Earth Planet. Int.* **169,** 41–48 (2008).
3. Helsley, C. E. & Steiner, M. B. Evidence for long intervals of normal polarity during Cretaceous period. *Earth Planet. Sci. Lett.* **5,** 325–332 (1969).
4. Biggin, A. J., van Hinsbergen, D. J. J., Langereis, C. G., Straathof, G. B. & Deenen, M. H. L. Geomagnetic secular variation in the Cretaceous normal superchron and in the Jurassic. *Phys. Earth Planet. Int.* **169,** 3–19 (2008).
5. Granot, R., Tauxe, L., Gee, J. S. & Ron, H. A view into the Cretaceous geomagnetic field from analysis of gabbros and submarine glasses. *Earth Planet. Sci. Lett.* **256,** 1–11 (2007).
6. Tarduno, J. A., Cottrell, R. D. & Smirnov, A. V. High geomagnetic intensity during the Mid-Cretaceous from Thellier analyses of single plagioclase crystals. *Science* **291,** 1779–1783 (2001).
7. Cronin, M., Tauxe, L., Constable, C., Selkin, P. & Pick, T. Noise in the quiet zone. *Earth Planet. Sci. Lett.* **190,** 13–30 (2001).
8. Tarduno, J. A. Brief reversed polarity interval during the Cretaceous normal polarity superchron. *Geology* **18,** 683–686 (1990).
9. Olson, P. L., Coe, R. S., Driscoll, P. E., Glatzmaier, G. A. & Roberts, P. H. Geodynamo reversal frequency and heterogeneous core-mantle boundary heat flow. *Phys. Earth Planet. Int.* **180,** 66–79 (2010).
10. Linder, J. & Gilder, S. A. Geomagnetic secular variation recorded by sediments deposited during the Cretaceous normal superchron at low latitude. *Phys. Earth Planet. Int.* **187,** 245–260 (2011).
11. Bouligand, C., Dyment, J., Gallet, Y. & Hulot, G. Geomagnetic field variations between chrons 33r and 19r (83–41 Ma) from sea-surface magnetic anomaly profiles. *Earth Planet. Sci. Lett.* **250,** 541–560 (2006).
12. Cande, S. C. & Kent, D. V. Ultrahigh resolution marine magnetic anomaly profiles: A record of continuous paleointensity variations? *J. Geophys. Res.* **97,** 15075–15083 (1992).
13. Gee, J. S., Cande, S. C., Hildebrand, J. A., Donnelly, K. & Parker, R. L. Geomagnetic intensity variations over the past 780 kyr obtained from near-seafloor magnetic anomalies. *Nature* **408,** 827–832 (2000).
14. Pouliquen, G., Gallet, Y., Patriat, P., Dyment, J. & Tamura, C. A geomagnetic record over the last 3.5 million years from deep-tow magnetic anomaly profiles across the Central Indian Ridge. *J. Geophys. Res.* **106,** 10941–10960 (2001).
15. Honsho, C. *et al.* Magnetic structure of a slow spreading ridge segment: Insights from near-bottom magnetic measurements on board a submersible. *J. Geophys. Res.* **114,** B05101 (2009).
16. Bird, D. E., Hall, S. A., Burke, K., Casey, J. F. & Sawyer, D. S. Early Central Atlantic Ocean seafloor spreading history. *Geosphere* **3,** 282–298 (2007).
17. Tucholke, B. E. & Schouten, H. Kane fracture zone. *Mar. Geophys. Res.* **10,** 1–39 (1988).
18. Gee, J. S. & Kent, D. V. in *Treatise on Geophysics Vol. 5, Geomagnetism* (ed. Kono, M.) 455–507 (Elsevier, 2007).
19. Bowers, N. E., Cande, S. C., Gee, J. S., Hildebrand, J. A. & Parker, R. L. Fluctuations of the paleomagnetic field during chron C5 as recorded in near-bottom marine magnetic anomaly data. *J. Geophys. Res.* **106,** 26379–26396 (2001).
20. Granot, R., Cande, S. C. & Gee, J. S. The implications of long-lived asymmetry of remanent magnetization across the North Pacific fracture zones. *Earth Planet. Sci. Lett.* **288,** 551–563 (2009).
21. Tauxe, L. & Yamazaki, T. in *Treatise on Geophysics Vol. 5, Geomagnetism* (ed. Kono, M.) 509–563 (Elsevier, 2007).
22. Driscoll, P. & Olson, P. Superchron cycles driven by variable core heat flow. *Geophys. Res. Lett.* **38,** L09304 (2011).
23. Haq, B. U., Hardenbol, J. & Vail, P. R. Chronology of fluctuating sea levels since the Triassic. *Science* **238,** 1156–1167 (1987).
24. Seton, M., Gaina, C., Müller, R. D. & Heine, C. Mid-Cretaceous seafloor spreading pulse: Fact or fiction? *Geology* **37,** 687–690 (2009).
25. Cogné, J-P., Humler, E. & Courtillot, V. Mean age of oceanic lithosphere drives eustatic sea-level change since Pangea breakup. *Earth Planet. Sci. Lett.* **245,** 115–122 (2006).
26. Müller, R. D., Sdrolias, M., Gaina, C. & Roest, W. R. Age, spreading rates, and spreading asymmetry of the world's ocean crust. *Geochem. Geophys. Geosyst.* **9,** Q04006 (2008).
27. Finlay, C. C. *et al.* International geomagnetic reference field: The eleventh generation. *Geophys. J. Int.* **183,** 1216–1230 (2010).
28. Hussenoeder, S. A., Tivey, M. A. & Schouten, H. Direct inversion of potential fields from an uneven track with application to the Mid-Atlantic Ridge. *Geophys. Res. Lett.* **22,** 3131–3134 (1995).
29. Besse, J. & Courtillot, V. Apparent and true polar wander and the geometry of the geomagnetic field over the last 200 Myr. *J. Geophys. Res.* **107,** 2300 (2002).
30. Biggin, A. J., McCormack, A. & Roberts, A. Paleointensity database updated and upgraded. *EOS Trans. AGU* **91,** 15 (2010).

Acknowledgements

We thank the captains and crews of RV *Le Suroît* and the scientific parties for their dedication at sea on cruises Magofond 3 (2005) and Magofond 3b (2008). IPGP, CNRS-INSU, IFREMER and GENAVIR are gratefully acknowledged for their financial and technical support at various stages of the project. R.G. was supported by fellowships given by IPGP and the city of Paris. This is IPGP contribution 3255.

Author contributions

J.D. and Y.G. designed and led data acquisition experiments. R.G. processed the data, interpreted them, and wrote the paper with contributions from both co-authors.

Additional information

The authors declare no competing financial interests. Supplementary information accompanies this paper on www.nature.com/naturegeoscience. Reprints and permissions information is available online at www.nature.com/reprints. Correspondence and requests for materials should be addressed to R.G.